Euler Procedure for Three-Dimensional Transonic Wall Interference

Magdi H. Rizk* and Donald R. Lovell†
Flow Research Inc., Kent, Washington
and
Timothy J. Baker‡
Princeton University, Princeton, New Jersey

Based on an optimization formulation, a procedure has been developed to evaluate Mach number and angle-of-attack corrections. The Euler equations are assumed to be the flow governing equations. To obtain efficient solutions for the optimization problem, the iterative solutions for the flow variables and the design parameters are simultaneously updated. In addition to the model lift and geometry, the procedure requires pressure measurements near the tunnel walls. The tunnel boundary conditions are based on the introduction of Riemann invariants for a one-dimensional flow normal to the boundary. Computations are performed to verify that the errors introduced by this approximate boundary-condition formulation are acceptably small. The correction scheme is applied to an aircraft configuration in an open jet. The results indicate that the optimization scheme is highly efficient with the rate of convergence of the flow solution nearly equal to the corresponding rate of a regular analysis problem.

Nomenclature

A_α = upper allowed limit for angle-of-attack increment
a = speed of sound normalized by $\hat{a}_\infty$
$\hat{a}_\infty$ = freestream speed of sound
$\hat{C}$ = characteristic length
C_α = proportionality constant for the chord method
c_1 = incrementing factor for optimization scheme
c_2 = decrementing factor for optimization scheme
E = total energy normalized by $\hat{a}_\infty^2$
E_L = defined in Eq. (8a)
E_M = defined in Eq. (11)
E_α = defined in Eq. (9b)
$\boldsymbol{f}$ = defined in Eq. (2)
$\boldsymbol{g}$ = defined in Eq. (2)
H = total enthalpy normalized by $\hat{a}_\infty^2$
$\boldsymbol{h}$ = defined in Eq. (2)
L = lift coefficient
M = Mach number
n = coordinate normal to the boundary and pointing outward
$\boldsymbol{n}$ = unit vector normal to the computational domain boundary and pointing out of the computational domain
$\boldsymbol{P}_F$ = $(\alpha_F, M_{\infty F})$
$\boldsymbol{P}_T$ = $(\alpha_T, M_{\infty T})$
p = pressure normalized by $\hat{p}_\infty$
$\hat{p}_\infty$ = freestream pressure
q_n = velocity component normal to the computational domain boundary and pointing out of the computational domain normalized by $\hat{u}_\infty$
q_τ = projection of the velocity to the computational domain boundary normalized by $\hat{u}_\infty$
R = Riemann invariant
$R_{\max}$ = maximum residual
u = velocity component in the freestream direction normalized by $\hat{u}_\infty$
$\hat{u}_\infty$ = freestream velocity
v = velocity component vertically upward normalized by $\hat{u}_\infty$
$\boldsymbol{W}$ = $(\rho, \rho u, \rho v, \rho w, \rho E)$
w = velocity component normal to the model plane of symmetry normalized by $\hat{u}_\infty$
x,y,z = Cartesian coordinates normalized by $\hat{C}$
α = angle of attack
γ = ratio of specific heats
ΔM = Mach number correction
$\Delta\alpha$ = angle-of-attack correction
$\delta M_{\infty F}$ = Mach number iterative increment
$\delta\alpha$ = angle-of-attack iterative increment
ρ = density normalized by $\hat{\rho}_\infty$
$\hat{\rho}_\infty$ = freestream density

Subscripts

B = tunnel boundary
E = values at the interior cells adjacent to the boundary
e = measured tunnel condition
F = computed free-air condition
f = corrected conditon
T = computed tunnel condition
∞ = freestream condition

Superscripts

n = number of iterations
$*$ = optimum value

Received Feb. 16, 1988; revision received May 21, 1988.

*Senior Research Scientist, Applied Mechanics Division; currently with Sverdrup Technology, Inc., Elgin Air Force Base, Florida. Member AIAA.
†Scientific Programmer, Applied Mechanics Division.
‡Research Scientist, Department of Mechanical and Aerospace Engineering. Member AIAA.

Introduction

AIRCRAFT models are tested in wind tunnels to study their aerodynamic properties and to estimate their performance qualities. Because of wall interference effects, however, the properties observed in the wind tunnel differ from those

observed under free-air conditions. To estimate correctly the free-air performance of the tested models and to achieve the maximum benefit from wind-tunnel tests for design improvements, it is necessary to determine the wall interference effects and to correct for them accurately.

The classical procedure[1] for correcting wall interference effects is based on linear theory. The model is represented by singularities deduced from the model geometry and measured forces. Although the classical wall interference theory provides insight into the features of wall interference, it does not produce sufficiently accurate formulas for practical use. Its limitations include the modeling of the ventilated tunnel walls by the general homogeneous wall boundary conditions; the assumption that the model is small compared to the tunnel size; the assumption of an infinitely long test section; and the neglect of transonic flow effects.

Over the past decade, two-dimensional wall interference correction and assessment procedures that eliminate some of the limitations of the classical theory have been developed. These methods are summarized by Mokry et al.[2] Many of these procedures replace the inaccurate homogeneous wall boundary conditions with measured flow properties. This eliminates a major source of error associated with the classical approach. The use of measured boundary data was extended to three-dimensional wall interference correction procedures by Mokry,[3] Mokry et al.,[4] Rizk and Smithmeyer,[5] Rizk,[6] Rizk and Murman,[7] and Moses.[7] These methods, with the exception of that by Rizk and Murman,[7] address the subsonic problem. The approach of Rizk and Murman is suitable for transonic wall interference corrections. However, a number of simplifying approximations made there need to be replaced by more accurate formulations to allow the prediction of wall interference effects for real test models. These approximations include the use of the transonic small-disturbance equations, the use of linearized boundary conditions, and the use of a Cartesian computational mesh.

In the correction procedure presented here, the Euler equations are assumed to be the flow governing equations, and body-fitted coordinates are used to apply accurately the surface boundary conditions. In order to obtain solutions efficiently, a multigrid strategy, together with a multistage time-stepping scheme, is used to advance the iterative solutions. The procedure is based on an optimization formulation in which the corrected Mach number and angle of attack are those optimum values that minimize the Mach number difference on the model surface in the wind tunnel and in free air while matching the lift. The correction procedure presented here is an extension of the recently developed two-dimensional procedure of Rizk et al.[9] to three-dimensional configurations.

Formulation

Flow Governing Equations

The correction procedure is divided into two basic steps. In the first and second steps, the flow is numerically simulated about the model in the wind tunnel and in free air, respectively. The Euler equations

$$\boldsymbol{D}(\boldsymbol{W};M_\infty) \equiv \partial/\partial x[\boldsymbol{f}(\boldsymbol{W};M_\infty)] + \partial/\partial y[\boldsymbol{g}(\boldsymbol{W};M_\infty)] + \partial/\partial z[\boldsymbol{h}(\boldsymbol{W};M_\infty)] = 0 \tag{1}$$

are assumed to be the flow governing equations, where

$$\boldsymbol{W} = \begin{bmatrix} \rho \\ \rho u \\ \rho v \\ \rho w \\ \rho e \end{bmatrix}, \quad \boldsymbol{f} = \begin{bmatrix} \rho u M_\infty \\ \rho u^2 M_\infty^2 + \frac{p}{\gamma} \\ \rho u v M_\infty^2 \\ \rho u w M_\infty^2 \\ \rho u H M_\infty \end{bmatrix},$$

$$\boldsymbol{g} = \begin{bmatrix} \rho v M_\infty \\ \rho v u M_\infty^2 \\ \rho v^2 M_\infty^2 + \frac{p}{\gamma} \\ \rho v w M_\infty^2 \\ \rho v H M_\infty \end{bmatrix}, \quad \boldsymbol{h} = \begin{bmatrix} \rho w M_\infty \\ \rho w u M_\infty^2 \\ \rho w v M_\infty^2 \\ \rho w^2 M_\infty^2 + \frac{p}{\gamma} \\ \rho w H M_\infty \end{bmatrix} \tag{2}$$

The coordinate system is such that the x and y axes lie in the model plane of symmetry, where the x axis is the horizontal axis pointing in the flow direction and the y axis is vertically upward. The z axis is the horizontal axis normal to the plane of symmetry. The total energy E and total enthalpy H normalized by the square of the freestream speed of sound, are given by

$$H = E + p/\gamma\rho$$

$$E = p/[\gamma(\gamma-1)\rho] + \tfrac{1}{2}M_\infty^2(u^2+v^2+w^2)$$

where $p = \rho a^2$. The normalization used here allows the freestream Mach number M_∞ to appear explicitly in the governing equations. This explicit appearance is a requirement of the correction scheme.

The Euler equations are solved subject to solid-wall boundary conditions at the model surface and to outer boundary conditions applied at the outer boundaries of the computational domain. The outer boundary conditions differ in the first step of the correction procedure, where the wind-tunnel flow is simulated, and in the second step of the correction procedure, where the free-air flow is simulated.

Outer Boundary Conditions for Wind-Tunnel Simulation

Following Ref. 10, the treatment of the tunnel boundary conditions, in the first step of the correction procedure, and the free-air far-field boundary conditions, in the second step of the procedure, is based on the introduction of the Riemann invariants for a one-dimensional flow normal to the boundary. The free-air far-field boundary conditions used here are given in Ref. 10.

In the first step of the correction procedure, the system of equations given as Eq. (1) is solved subject to an experimentally measured pressure distribution on the upper, lower, and side planes of a rectangular parallelepiped and to appropriate boundary conditions (either experimental or theoretical) on the end planes of the parallelepiped, upstream and downstream of the model. The upper, lower, and side planes of the parallelepiped are assumed to be close to the tunnel walls but outside the boundary-layer region. It is this parallelepiped that defines the boundaries of the computational domain for the tunnel simulation. Boundary conditions at the end planes of the computational domain, based on experimental measurements, are derived in Ref. 11. Using present experimental techniques, it is not practical to obtain experimental measurements at the upstream and downstream boundaries. In the present work, boundary conditions similar to those of the far field in free air are applied at the upstream and the downstream boundaries.

At the upper, lower, and side boundaries, the Riemann invariant corresponding to the outgoing characteristic introduces the following relation between q_{nB} and a_B

$$R_B \equiv M_\infty q_{nB} + \left(\frac{2}{\gamma-1}\right)a_B = R_E \equiv M_\infty q_{nE} + \left(\frac{2}{\gamma-1}\right)a_E \tag{3}$$

The use of Eq. (3) for flows that are not one-dimensional is an approximation. In three-dimensional flows, R_B and R_E are related at steady state by

$$R_B = R_E + \frac{(n_B - n_E)G}{q_n + a} \tag{4}$$

where

$$G = -M_\infty^2 \boldsymbol{q}_\tau \cdot \nabla_\tau q_n - a/\rho[M_\infty \nabla_\tau \cdot (\rho \boldsymbol{q}_\tau)]$$

The subscript τ in the operator ∇_τ indicates that the derivative associated with the coordinate normal to the boundary plane in the operator ∇ has been eliminated; thus, ∇_τ is a two-dimensional operator operating within the boundary plane. The error introduced by using Eq. (3) instead of Eq. (4) is given by the last term in Eq. (4). This error is expected to be small provided the derivatives of the solution along the boundary are small and provided the distance between the boundary and the center of the adjacent mesh cells is small.

The normal velocity component q_{nB} is evaluated from Eq. (3) with

$$a_B = [p_B/\rho_E]^{1/2}[p_E/p_B]^{1/2\gamma} \tag{5}$$

The equation for the total enthalpy is then used to evaluate $q_{\tau B}$, which is given by

$$q_{\tau B} = \{2/M_\infty^2[H_\infty - (1/\gamma - 1)a_B^2] - q_{nB}^2\}^{1/2} \tag{6}$$

The total energy is evaluated by the relation

$$E_B = H_\infty - (a_B^2/\gamma) \tag{7}$$

Equation (6) gives the magnitude of the velocity projection onto the boundary plane. In order to solve the Euler equations, a knowledge of the three velocity components is required at the boundaries. The vector $\boldsymbol{q}_{\tau B}$ may be resolved into its two components if its direction is known. This direction may be measured experimentally at the boundary planes; otherwise, simplified estimates must be used.

Correction Procedure

In the first step of the correction procedure, an equivalent angle of attack α_T is determined such that the tunnel-computed lift coefficient L_T matches the measured lift coefficient L_e of the tested model. Let $\boldsymbol{P}_T$ denote the parameters $(\alpha_T, M_{\infty T})$. The problem solved in this step may be stated as follows: Find α_T subject to the constraint

$$E_L(\boldsymbol{P}_T; \boldsymbol{W}_T) \equiv \frac{L_T(\boldsymbol{P}_T; \boldsymbol{W}_T) - L_e}{L_e} = 0 \tag{8a}$$

with $\boldsymbol{W}_T$ satisfying the equation

$$\boldsymbol{D}(\boldsymbol{W}_T; M_{\infty T}) = 0 \tag{8b}$$

Although α_T, the first component of $\boldsymbol{P}_T$, is determined in this step, the second component $M_{\infty T}$ is set equal to the measured value $M_{\infty e}$.

In the second step of the correction procedure, the free-air flow is numerically simulated. The free-air angle of attack α_F and the Mach number $M_{\infty F}$ are determined in this step. Let $\boldsymbol{P}_F$ denote the parameters $(\alpha_F, M_{\infty F})$. The problem solved in this step is an optimization problem in which $\boldsymbol{P}_F$ is the vector of design parameters. The optimum value of $\boldsymbol{P}_F$, $\boldsymbol{P}_F^*$, is determined such that the objective function E_M satisfies the condition

$$E_M(\boldsymbol{P}_F^*; \boldsymbol{W}_F) = \min_{\boldsymbol{P}_F} E_M(\boldsymbol{P}_F; \boldsymbol{W}_F) \tag{9a}$$

subject to the constraint

$$E_\alpha(\boldsymbol{P}_F; \boldsymbol{W}_F) \equiv \frac{L_F(\boldsymbol{P}_F; \boldsymbol{W}_F) - L_T(\boldsymbol{P}_T; \boldsymbol{W}_T)}{L_T(\boldsymbol{P}_T; \boldsymbol{W}_T)} = 0 \tag{9b}$$

with $\boldsymbol{W}_F$ satisfying the equation

$$\boldsymbol{D}(\boldsymbol{W}_F; M_{\infty F}) = 0 \tag{10}$$

The objective function E_M, which is minimized in the problem, is given by

$$E_M \equiv \frac{\int (M_F - M_T)^2 \, ds}{\int M_T^2 \, ds} \tag{11}$$

This is a measure of the Mach number difference on the model surface in the tunnel and in free air. The integrals are taken over the model surface. In Eq. (9b), L_F is the free-air calculated lift coefficient.

The Mach number and angle-of-attack corrections are calculated from the relations

$$\Delta M = M_{\infty F} - M_{\infty T} \qquad \Delta\alpha = \alpha_F - \alpha_T \tag{12}$$

and the corrected Mach number and angle of attack are then found from the relations

$$M_{\infty f} = M_{\infty e} + \Delta M \qquad \alpha_f = \alpha_e + \Delta\alpha \tag{13}$$

An estimate of the accuracy of the wall interference corrections is given by the value of E_M. If E_M exceeds an acceptable value, the data must be considered as uncorrectable. If an adaptive tunnel is available, it may be used to reduce the wall interference in this case.

Numerical Approach

The objective of the correction procedure is to determine the parameters α_T, α_F, and $M_{\infty F}$. In order to determine these parameters, it is necessary to determine the flow solution $\boldsymbol{W}$. The procedure for obtaining the solution $\boldsymbol{W}$ for the Euler equations in a regular analysis problem is an iterative procedure in which $\boldsymbol{W}$ is repeatedly updated until convergence is achieved. The approach used here follows that used in determining the analysis problem solution with the exception of allowing the parameters α_T, α_F, and $M_{\infty F}$ to be updated as $\boldsymbol{W}$ is updated so that convergence is achieved for the flow solution and the parameters α_T, α_F, and $M_{\infty F}$ simultaneously. The flow solver is based on a finite-volume discretization and uses a multigrid strategy together with a multistage time-stepping scheme to advance the flow solution to a steady state as rapidly as possible. The finite-volume Euler method used here was first developed in its basic form by Jameson et al.[12] Subsequent improvements include the incorporation of a multigrid strategy[13] and the extension of the method to treat complex three-dimensional configurations using a C-H mesh.[10,14,15] Details of the dissipative terms, the multistage schemes, and the multigrid method are given in Refs. 10, 12, and 14. A description of the mesh used in the computations follows.

Mesh Generation

The construction of a mesh around an aircraft-like configuration inside a rectangular wind tunnel must ensure that mesh lines coincide with wind-tunnel walls as well as the aircraft surface. This requirement is most readily accommodated by using an H-H mesh. The generation of an H mesh is first described for a two-dimensional airfoil section. For a three-dimensional wing, an H mesh is generated for each section; thus, the three-dimensional H-H mesh can be built up from a series of two-dimensional meshes. The two-dimensional mesh is generated by a mapping procedure based on the combination of a conformal parabolic mapping together with a shearing to create a mesh that is mildly nonorthogonal. The introduction of a body is accomplished by a further series of mappings. This approach is similar to that described in Baker,[15] where a sequence of transformations was used to generate a C-H mesh around an aircraft-like configuration.

H-Mesh Mapping for an Airfoil

Let (x,y) be the Cartesian coordinates of a point in physical space and define a complex variable $\xi = x + iy$. Let ξ_o repre-

sent a singular point located just inside the airfoil leading edge. Now define a new complex variable $\zeta = X + iY$, corresponding to a point (X,Y) in mapped space, by the square-root mapping

$$\zeta = k(\xi - \xi_o)^{1/2} \tag{14a}$$

where k is a constant scaling factor. Setting $\xi - \xi_o = re^{i\theta}$, then this mapping can be rewritten as

$$\zeta = kr^{1/2}e^{i\theta/2} \tag{14b}$$

If a branch cut is taken along the line Im $(\xi - \xi_o) = 0$, Re $(\xi - \xi_o) > 0$, it is found that the physical space is mapped into the region $Y \geq 0$ with the airfoil surface transformed into a shallow bump.

Now consider a Cartesian mesh in physical space with stretching applied in the x and y directions to cluster points near the airfoil. The square-root mapping will transform these mesh lines into two families of hyperbolas. Now deform the mesh lines in mapped space so that the X axis is displaced to coincide with the airfoil surface, Thus, if $S(X)$ represents the airfoil shape in mapped space, the shearing transformation

$$X' = X$$
$$Y' = Y + S(X) \tag{15}$$

is applied to all mesh points (i.e., those points represented by the intersections of the mesh lines). The mapping procedure can now be inverted to obtain the conforming H mesh in physical space

$$\xi' = \xi_o + \left(\frac{1}{k^2}\right)\zeta'^2$$

where $\zeta' = X' + iY'$. This can be written as

$$x' = x_o + \frac{1}{k^2}\{X^2 - [Y + S(X)]^2\}$$
$$y' = y_o + \frac{2}{k^2}X[Y + S(X)] \tag{16}$$

As it stands, the H mesh generated by the procedure will be relatively sparse near the airfoil's leading edge. To concentrate points close to the leading edge, a technique first suggested by Pelz and Steinhoff[16] is employed. When mapping the Cartesian mesh, the square-root mapping of Eq. (14b) is replaced by

$$\zeta = kf(r)e^{i\theta/2} \tag{17}$$

where

$$f(r) = \frac{r}{\sqrt{r} + \varepsilon}$$

Note that $f(r) \sim r$ when $r \ll \varepsilon$ and $f(r) \sim \sqrt{r}$ when $r \gg \varepsilon$. Thus, the mapping given by Eq. (17) introduces a variable scaling that reduces to Eqs. (14) in the far field but has the effect of pulling points closer to the origin in the mapped space than would be the case with the unmodified mapping. The inversion is carried out with the original form of Eq. (16) producing an H mesh that conforms with an airfoil surface and concentrates points near the leading edge.

H-H Mesh for a Wing

Now consider a three-dimensional space with a point defined by the Cartesian coordinates (x,y,z). The square-root mapping is generalized to the following form:

$$k^2(z)[x - x_o(z)] = X^2 - Y^2$$
$$k^2(z)[y - y_o(z)] = 2XY$$
$$z = Z$$

where the singular line (x_o,y_o) and scaling parameter k are now functions of the spanwise coordinate z.

The mapping procedure is a straightforward extension of the H-mesh mapping for an airfoil section. A Cartesian mesh is defined in physical space with an appropriate stretching of points in the x, y, and z directions. These points, considered section by section, are then passed through the square-root mapping and displaced if their images under the mapping lie above the mapped wing surface. The sheared mesh in mapped space is transformed back to physical space where it forms an H-H mesh that conforms with the wing surface. The mapping adjustment defined by Eq. (17) is applied to concentrate points close to the wing's leading edge.

Wing/Body Configuration

The introduction of a body can be accomplished in the manner described in Ref. 15 with some modifications necessary to allow for the use of an H mesh rather than a C mesh in each spanwise section.

By first mapping the body into the symmetry plane $z = 0$, it is possible to reduce the problem to a wing-alone case. This can be achieved by using a combination of a Joukowski mapping plus shearing. Suppose that $R(x)$ is half the diameter of the body profile and $y_c(x)$ is the position of the body centerline. Now define the transformation taking the point (x,y,z) into (x',y',z') in the following way:

$$x' = x$$
$$y' = (y - y_c)\left[1 + \frac{R^2}{(y - y_c)^2 + z^2}\right]$$
$$z' = z\left[1 - \frac{R^2}{(y - y_c)^2 + z^2}\right]$$

For a body with a circular cross section, this maps each body section into the $z' = 0$ plane. For general shapes, however, this mapping takes each body section into a shallow bump, and a shearing can again be used to complete the mapping into the $z' = 0$ plane. A Cartesian mesh in this intermediate space can be deformed to produce an H-H mesh that conforms with each section of the distorted wing surface. Inversion of the body mapping then creates an H-H mesh around the wing/body combination.

It is desirable to have one mesh line coincide with the body crestline. This can be achieved over most of the body, although it is necessary to allow the mesh line to break away from the body at a point just downstream of the nose and, likewise, at a point just upstream of the rear of the body. Under the body mapping, the body crestline maps to a line profile on the $z' = 0$ plane, which in turn maps to a curve in the half plane $Y \geq 0$, $Z = 0$. If this crestline is followed through the mapping sequence, the mesh lines can be further deformed in the mapped space (X,Y,Z) to change smoothly from a line that coincides with the mapped wing root section to one that coincides with most of the mapped body profile.

Although the free-air computational mesh does not require that its outer boundary mesh surfaces conform to a specific shape, the wind-tunnel computational mesh requires that they be planar so that the centers of the outer boundary mesh cells coincide with the positions of the sides of the parallelepiped at which the experimental pressure data are measured. Mesh shearing is, therefore, applied in the physical domain to achieve this requirement. The mesh spacing requirements for a free-air mesh and a tunnel mesh differ. The free-air solution has its largest gradients near the model surface, requiring a relatively fine mesh there. As one moves away from the model, these gradients diminish. A computational mesh that is increasingly stretched as the outer boundaries are approached is therefore appropriate for free-air computations. In the tunnel, the flow solution near the model has mesh requirements similar to those in free air. However, the solution as the tunnel boundary is approached is expected to have higher mesh resolution require-

ments than that of free air, because of the tunnel constraint. In addition, the one-dimensional characteristic equations applied there are approximate equations. The errors introduced by these equations increase as the mesh spacing is increased in the direction normal to the boundary as indicated by Eq. (4).

In the present work, the flow solutions at the model surface in the tunnel and in free air are generally close. The correction procedure attempts to make these two solutions as close as possible. The decisions for making Mach number and angle-of-attack correction in the correction scheme are based on comparing these two solutions. It is therefore essential to have equivalent computational meshes in the tunnel and in free air at both the model surface and in the region surrounding the model surface, where the two solutions are expected to be close, to minimize relative truncation effects. Similar solutions produced on similar computational meshes will produce similar truncation errors that will tend to cancel each other in the correction procedure. The free-air mesh can be chosen to coincide with the tunnel mesh in their overlapping region; however, increased computational efficiency can be achieved by having the two meshes deviate as the tunnel boundary position is approached, since resolution requirements for free-air computations are lower than those for wind-tunnel computations there.

Correction Scheme

Step 1—Wind-Tunnel Simulation

The goal in this step is to determine the value of the model angle of attack α_T that causes the model computed lift coefficient L_T to be equal to the experimental value L_e. In this step a solution for the wind-tunnel flowfield is obtained. The flowfield solution is obtained iteratively in a manner similar to that used for solving an analysis problem, with the exception of allowing α_T to vary as the computation progresses. Prior to the $(n+1)$th iterative step, in which the flow solution is updated, α_T is updated so that the value used in this step is α_T^{n+1}:

$$\alpha_T^{n+1} = \alpha_T^n + \delta\alpha_T^{n+1} \tag{18}$$

The increment $\delta\alpha_T^{n+1}$ is determined by the chord method and is given by

$$\delta\alpha_T^{n+1} = -\frac{E_L^n}{|E_L^n|}[\min(C_\alpha|E_L^n|, A_\alpha)] \tag{19}$$

where

$$E_L^n = E_L(\alpha_T^n, M_{\infty T}; \boldsymbol{W}_T^n)$$

and A_α and C_α are positive constants. The constant A_α sets an upper limit on the magnitude of $\delta\alpha_T^{n+1}$.

Step 2—Free-Air Simulation

The goal in this step is to determine the values for the model angle-of-attack α_F and the free-air Mach number $M_{\infty F}$ that minimize the objective function E_M subject to the lift constraint given in Eq. (9b). A search must, therefore, be conducted in the design parameter space $(\alpha_F, M_{\infty F})$ for the optimum solution. The optimization scheme used in the present work is that developed in Ref. 7. For fixed values of α_F and $M_{\infty F}$, let

$$\boldsymbol{W}_F^{n+1} = \psi(\boldsymbol{W}_F^n; \alpha_F, M_{\infty F}), \qquad n = 0,1,2\ldots \tag{20}$$

be the iterative solution for the analysis problem, where ψ denotes the solution obtained by applying the iterative (time-stepping) scheme for solving the Euler equations once using $\boldsymbol{W}_F^n$ as an initial guess. As for the analysis solution, obtaining the optimization solution requires the repeated application of Eq. (20) to update the flowfield. Although α_F and $M_{\infty F}$ are held fixed in the former case, they are allowed to vary in the latter. The scheme used to update these parameters follows.

Prior to the $(n+1)$th iterative step, in which the flow solution is updated, α_F and $M_{\infty F}$ are updated so that the values used in this step are α_F^{n+1} and $M_{\infty F}^{n+1}$:

$$\alpha_F^{n+1} = \alpha_F^n + \delta\alpha_F^{n+1} \tag{21a}$$

$$M_{\infty F}^{n+1} = M_{\infty F}^n + \delta M_{\infty F}^{n+1} \tag{21b}$$

The incremental values for the design parameters are given by

$$\delta\alpha_F^{n+1} = -\frac{E_\alpha^n}{|E_\alpha^n|}[\min(C_\alpha|E_\alpha^n|, A_\alpha)] \tag{22a}$$

$$\delta M_{\infty F}^{n+1} = \tfrac{1}{2}[c_1(\tau^{n+1}+1) + c_2(\tau^{n+1}-1)]\delta M_{\infty F}^n \tag{22b}$$

where

$$E_\alpha^n = E_\alpha(\boldsymbol{P}_F^n; \boldsymbol{W}_F^n) \tag{23}$$

$$\tau^{n+1} = -\frac{G^n \delta M_{\infty F}^n}{|G^n \delta M_{\infty F}^n|} \tag{24}$$

$$G^n = (E_M^n - E_M^{n-1})(e_M^n - e_M^{n-1}) \tag{25}$$

$$E_M^n = E_M(\boldsymbol{P}_F^n; \boldsymbol{W}_F^n) \tag{26}$$

$$e_M^n = e_M(\boldsymbol{P}_F^n; \boldsymbol{W}_F^n) = \frac{\int (M_F - M_T)\,\mathrm{d}s}{\int M_T\,\mathrm{d}s} \tag{27}$$

The updated values of α_F and $M_{\infty F}$ are used to calculate the new flow iterative solution $\boldsymbol{W}_F^{n+1}$ by

$$\boldsymbol{W}_F^{n+1} = \psi(\boldsymbol{W}_F^n; \alpha_F^{n+1}, M_{\infty F}^{n+1}) \tag{28}$$

Results and Discussion

The correction procedure was applied to a wing/body combination consisting of an ONERA M6 wing, with a wing span and maximum chord of 2.4 and 0.6737 unit lengths, respectively, mounted on a cylindrical body of 0.2-unit-length radius. The model was assumed to be tested in an open jet with zero pressure perturbations along its boundaries. The tunnel height and width considered were 2.0 and 4.0 unit lengths, respectively. The computational domain consisted of half the flowfield by including the plane of symmetry as one of its boundaries. The computational parameters $\delta M_{\infty F}^0$, c_1, c_2, C_α, and A_α were assigned the values of 0.005, 1.2, 0.6, 0.3, and 0.2, respectively. In all computations, the initial guess for the flow solution was set equal to freestream conditions.

Both the wind-tunnel and the free-air outer boundary conditions were derived using the Riemann invariants for a one-dimensional flow. The error introduced by this formulation is expected to affect the flow solution near the model. This effect, however, is expected to be stronger in the case of the wind-tunnel simulation, for which the boundary conditions are applied in the near field, than in the case of the free-air simulation, for which the boundary conditions are applied in the far field. The objective of the following computation is to verify that the errors introduced by applying the present tunnel boundary conditions do not exceed acceptable levels.

To test the wind-tunnel boundary conditions properly, it is necessary to have identical meshes within the wind-tunnel computational region for both the wind-tunnel computation and the free-air computation. The meshes used in this particular computation satisfied this condition. A $72 \times 24 \times 12$ mesh was used for the tunnel computation, whereas a $72 \times 40 \times 16$ mesh was used for the free-air computation. In this example, the measured tunnel pressure data were replaced by numerical solutions of the Euler equations simulating free-air flow conditions. In other words, an interference-free tunnel was assumed.

The exact solution for this example is known. It is given by $\Delta\alpha = \Delta M = 0$. The test conditions are given by $\alpha_e = 3.0$ deg, $M_{\infty e} = 0.84$, and $L_e = 0.2640$. In the first step of the correction procedure, the tunnel flow is computed and the angle of attack α_T is determined. The initial iterative guess for α_T was chosen to be given by $\alpha_T^0 = 2.0$ deg. The iterative histories for α_T and L_T are shown in Fig. 1. The lift coefficient L_T converges to the specified experimental value L_e, as shown in the figure, while the angle of attack is $\alpha_T = 3.012$ deg. The deviation of this value from the exact value is 0.012 deg. This deviation is due to the approximations introduced in the tunnel boundary conditions. In the second step of the correction procedure, the free-air flow is computed and the parameters α_F and $M_{\infty F}$ are determined. The initial iterative guesses for α_F and $M_{\infty F}$ were 5.012 deg and 0.8, respectively. The iterative histories for L_F and α_F are shown in Fig. 2, while the iterative history for $M_{\infty F}$ is shown in Fig. 3. The solutions determined in the second step of the correction procedure are given by $\alpha_F = 3.006$ deg and $M_{\infty F} = 0.840$. The corrections $\Delta\alpha$ and ΔM are, therefore, given by $\Delta\alpha = -0.006$ deg and $\Delta M = 0.000$. Although not identically zero, the errors in determining $\Delta\alpha$ and ΔM are acceptably small. This indicates that the present formulation of the tunnel boundary conditions is adequate.

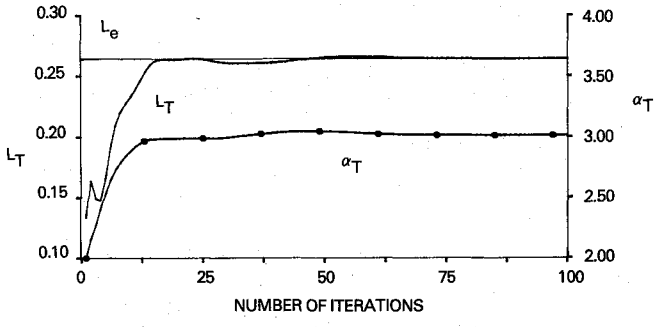

Fig. 1 Iterative histories for the wind-tunnel solutions (no wall interference).

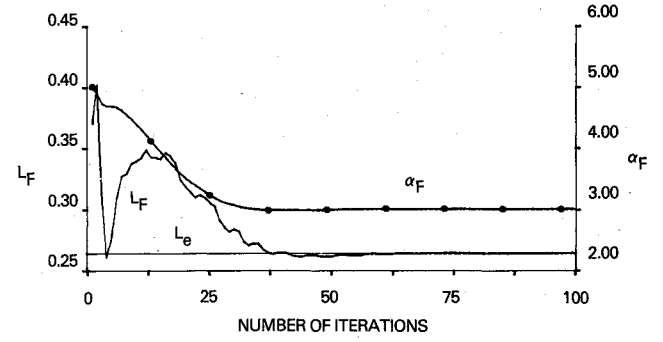

Fig. 2 Iterative histories for the free-air solutions (no wall interference).

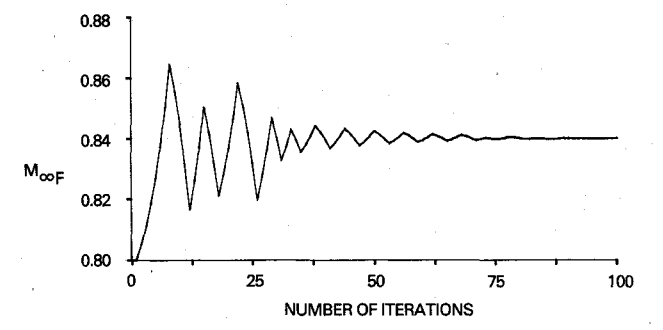

Fig. 3 Iterative history for $M_{\infty F}$ (no wall interference).

The correction procedure was applied to the model that was assumed to be tested in the open jet. A $72 \times 24 \times 12$ mesh was used for the tunnel computation, whereas a $72 \times 32 \times 12$ mesh was used for the free-air computation. In this example, the free-air mesh and the tunnel mesh were identical in a region bounded by the upper and lower tunnel walls and the wing tip. Beyond the wing tip, the meshes did not coincide. The experimental conditions were given by $M_{\infty e} = 0.84$, and $L_e = 0.20$. The first step for the correction procedure determined an α_T value of 2.777 deg. The iterative histories for α_T and L_T are shown in Fig. 4, while the maximum residual history is shown in Fig. 5. The second-step of the correction procedure determined α_F and $M_{\infty F}$ values given by $\alpha_F = 2.468$ deg and $M_{\infty F} = 0.833$. The angle-of-attack and Mach number corrections are, therefore, given by $\Delta\alpha = -0.309$ deg and $\Delta M = -0.007$. Figure 6 shows the iterative histories for α_F and L_F, while the iterative history for $M_{\infty F}$ is shown in Fig. 7. Figure 8 compares $R_{\max}$ for the second step in the correction procedure, in which W is updated in addition to α_F and $M_{\infty F}$, to $R_{\max}$ for the regular analysis solution, in which only W is updated while α_F and $M_{\infty F}$ are held fixed. The figure indicates that the convergence rates for the analyses and the correction schemes are comparable. The high-frequency oscillations apparent in the curve associated with the correction procedure are due to the

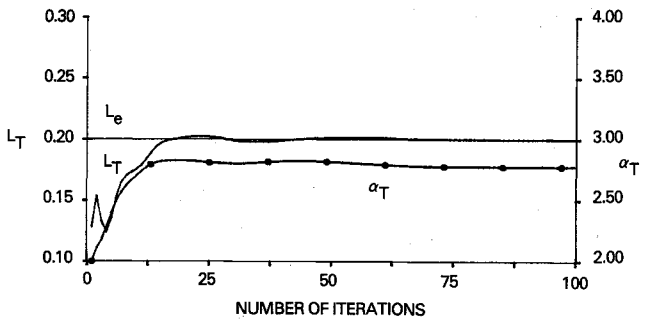

Fig. 4 Iterative histories for the wind-tunnel solution (free jet).

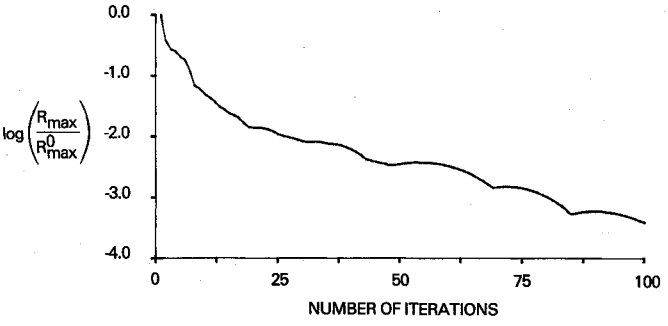

Fig. 5 Residual evolution history for the wind-tunnel solutions (free jet).

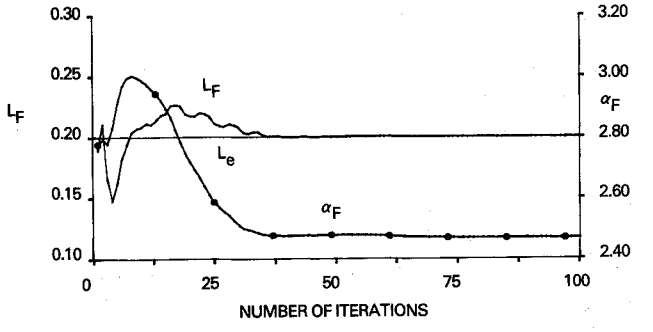

Fig. 6 Iterative histories for the free-air solutions (free jet).

introduction of perturbations in the flowfield as $M_{\infty F}$ is updated. The computational requirements for the free-air correction scheme and the analysis scheme were essentially the same, while the wind-tunnel computation required 50% more CPU time than the free-air computation. The relatively high computational cost in this case is due to the regeneration of the computational mesh at each iterative step. For the free-air computation, a single mesh is used. For the uncorrected free-air flow ($M_{\infty F} = 0.84$, $\alpha_F = 2.777$ deg), the values of L_F and E_M are given by $L_F = 0.235$, $E_M = 5.2 \times 10^{-6}$. For the corrected free-air flow ($M_{\infty F} = 0.833$, $\alpha_F = 2.468$ deg), these values are given by $L_F = 0.200$, $E_M = 6.92 \times 10^{-7}$. The corrections therefore achieved the goal of satisfying the lift constraint and of reducing the value of the objective function.

Until this point, E_M defined by Eq. (11) was used for two purposes. It was used as the objective function with the purpose of minimizing the Mach number difference on the model surface in the wind tunnel and in free air, and it was also used as a measure of the residual wall interference. When multicomponent models are tested, the wall interference effects do not affect the different components in a uniform manner. It is possible to determine the residual wall interference, referred to here as E_{Mr}, for the different components by redefining the integrals in Eq. (11) to be taken over the surface of a particular component. It is also possible to determine the wall interference corrections that minimize the wall interference effects for a particular component by redefining the objective function, referred to here as E_{Mo}, so that the integrals in Eq. (11) are taken over the surface of the particular component.

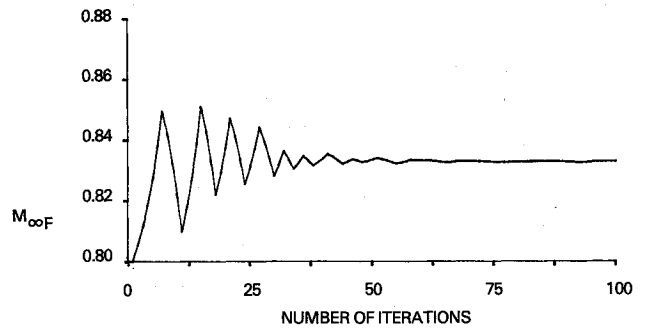

Fig. 7 Iterative history for $M_{\infty F}$ (free jet).

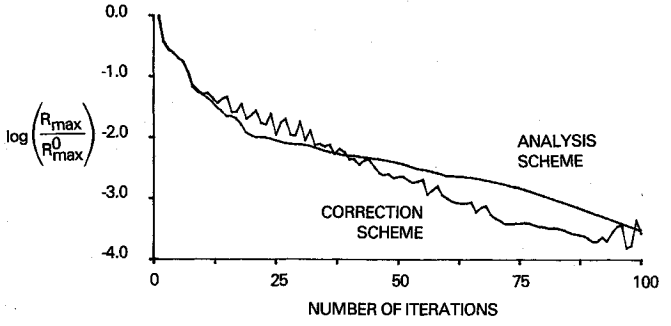

Fig. 8 Residual evolution histories for the correction problem and the analysis problem in free air (free jet).

Table 1 Residual wall interference

Component on which E_{Mo} is based	E_{Mr} (wing)	E_{Mr} (body)	E_{Mr} (model)
Wing	7.32×10^{-8}	6.65×10^{-7}	7.38×10^{-7}
Model	9.33×10^{-8}	5.99×10^{-7}	6.92×10^{-7}

Computations were performed in which the integrals in the objective function E_{Mo} were taken over the wing and the total model. Table 1 gives the residual wall interference for the different components for each of the cases. The table indicates that the residual wall interference for the wing, or the total model, attains its minimum value in the case in which the objective function integrals are taken over the wing, or the total model.

Although the wall interference correction procedure does require the numerical simulation of the flow about the test model, the goal here is to predict $\Delta\alpha$, ΔM, and E_M and not to compute aerodynamic properties of the model. These properties are to be obtained experimentally. We, therefore, expect the level of accuracy requirement for simulating the flowfield in the wall interference correction procedure to be less stringent than that for simulating the flowfield with the goal of studying the flowfield about the model. A finer computational mesh, for example, may be required in the second computation. Basic flow equation requirements may also differ. In the correction procedure presented here, the Euler inviscid flow equations are used to describe the flowfield. These equations describe the flow accurately everywhere except in the boundary-layer region where viscous effects are not negligible. A simple viscous correction was introduced by determining an inviscid equivalent angle of attack α_T in the first step of the correction procedure, such that the computed tunnel lift coefficient L_T matches the measured lift coefficient L_e. Increased levels of accuracy and complexity for the viscous correction may be introduced through the use of any one of a wide range of formulations.[17-19] For the correction procedure, it may not be necessary to do so. This, however, can only be determined by further testing of the procedure.

The wall interference correction procedure presented here determines the angle-of-attack correction $\Delta\alpha$ and the Mach number correction ΔM that minimize the difference between flow properties on the model surface when tested in the tunnel and in free air. A match between the flow properties in these two cases is not achievable if the freestream Mach number M_∞ and the model angle of attack α are the only two parameters allowed to vary. Consequently, the procedure used here does not completely correct for wall interference effects. There is a residual interference not accounted for by the Mach number and angle-of-attack corrections. If this residual, quantified by the error E_M, is small, then the corrections $\Delta\alpha$ and ΔM are sufficient to produce free-air conditions that nearly match the tunnel conditions. However, if the residual is large, then the corrections $\Delta\alpha$ and ΔM are not sufficient to produce free-air conditions that nearly match the tunnel test conditions. In this case, the data must be considered uncorrectable. When applying the correction procedure to experimental data, it is necessary to define a value for E_M as an upper limit for acceptable data.

The optimization scheme used here is that developed in Ref. 7. In the two-dimensional tests discussed in Ref. 9, with relatively large supersonic bubbles, this scheme did not converge properly. A second scheme that converges properly under all conditions was developed in Ref. 9. This new scheme, however, is less efficient and has larger computer memory requirements. The three-dimensional relief effect leads to favorable conditions for the operation of the scheme of Ref. 7. This is very advantageous, in view of the high cost of computations and the large computational memory requirements associated with the three-dimensional problems.

The main focus of this study has been on the numerical aspect of the transonic wall interference correction problem. Other aspects of the problem, not considered here, include the experimental aspect of making pressure measurements near the wind-tunnel walls, and the use of this experimental data to estimate the required boundary conditions for the numerical procedure through aerodynamic interpolation.[20]

Conclusions

The main elements of a transonic wind-tunnel wall interference correction procedure have been developed and tested. In the procedure, the corrected Mach number and angle of attack are those optimum values that minimize the Mach number difference on the model surface in the tunnel and in free air while matching the lift. An estimate of the correctability of the data, by varying the Mach number and the angle of attack, is provided by the procedure. The optimization scheme used here is based on updating the iterative solutions for the flow variables, the freestream Mach number, and the model angle of attack simultaneously. The results indicate that this scheme is highly efficient with the rate of convergence of the flow solution nearly equal to the corresponding rate for a regular analysis problem.

Acknowledgment

This work was sponsored by NASA Ames Research Center under Contract NAS2-12157.

References

[1] Garner, H. C., Rogers, E. W. E., Acum, W. E. A., and Maskell, E. C., "Subsonic Wind-Tunnel Wall Corrections," AGARDograph 109, Oct. 1966.

[2]Mokry, M., Chan, Y. Y., and Jones, D. J., "Two-Dimensional Wind-Tunnel Wall Interference," AGARDograph 281, Nov. 1983.

[3]Mokry, M., "Subsonic Wall Interference Corrections for Finite Length Test Sections Using Boundary Pressure Measurements," Paper 10, AGARD Fluid Dynamics Panel Specialists' Meeting on Wall Interference in Wind Tunnels, May 1982.

[4]Mokry, M., Digney, J. R., and Poole, R. J. D., "Doublet-Panel Method for Half-Model Wind-Tunnel Corrections," *Journal of Aircraft*, Vol. 24, May 1987, pp. 322–327.

[5]Rizk, M. H. and Smithmeyer, M. G., "Wind-Tunnel Wall Interference Corrections for Three-Dimensional Flows," *Journal of Aircraft*, Vol. 19, June 1982, pp. 465–472.

[6]Rizk, M. H., "Higher-Order Flow Angle Corrections for Three-Dimensional Wind-Tunnel Wall Interference," *Journal of Aircraft*, Vol. 19, Oct. 1982, pp. 893–895.

[7]Rizk, M. H. and Murman, E. M., "Wind-Tunnel Wall Interference Corrections for Aircraft Models in the Transonic Regime," *Journal of Aircraft*, Vol. 21, Jan. 1984, pp. 54–61.

[8]Moses, D. F., "Wind-Tunnel Wall Corrections Deduced by Iterating from Measured Wall Static Pressure," *AIAA Journal*, Vol. 21, Dec. 1983, pp. 1667–1673.

[9]Rizk, M. H., Lovell, D. R., and Baker, T. J., "Euler Procedure for Correcting Two-Dimensional Transonic Wind-Tunnel Wall Interference," *AIAA Journal* (to be published).

[10]Jameson, A. and Baker, T. J., "Solution of the Euler Equations for Complex Configurations," AIAA Paper 83-1929, July 1983.

[11]Rizk, M. H. and Lovell, D. R., "Two-Dimensional Transonic Wind-Tunnel Wall Interference Corrections Based on the Euler Equations," AIAA Paper 86-0124, Jan. 1986.

[12]Jameson, A., Schmidt, W., and Turkel, E., "Numerical Solutions of the Euler Equations by Finite-Volume Methods Using Runge-Kutta Time-Stepping Schemes," AIAA Paper 81-1259, June 1981.

[13]Jameson, A., "Solution of the Euler Equations for Two-Dimensional Transonic Flow by a Multigrid Method," Princeton Univ., Princeton, NJ, Dept. of Mechanical Aerospace Engineering, Rept. 1613, June 1983.

[14]Jameson, A. and Baker, T. J., "Multigrid Solution of the Euler Equations for Aircraft Configurations," AIAA Paper 84-0093, Jan. 1984.

[15]Baker, T. J., "Mesh Generation by a Sequence of Transformations," *Applied Numerical Mathematics*, Vol. 2, Dec. 1986, pp. 515–528.

[16]Pelz, R. and Steinhoff, J., "Multigrid ADI Solutions of the Transonic Full Potential Equation for Airfoils Mapped to Slits," *Proceedings of Symposium on Computers in Flow Prediction and Fluid Dynamics Experiments*, ASME, 1981, p. 27.

[17]Jou, W. -H. and Murman, E. M., "A Phenomenological Model for Displacement Thickness Effects of Transonic Shock Wave Boundary-Layer Interactions," Paper 15, *AGARD Conference Proceedings*, No. 291, 1980.

[18]Bauer, F., Garabedian, P. R., Korn, D. G., and Jameson, A., "Supercritical Wing Sections II," *Lecture Notes in Economics and Mathematical Systems*, No. 108, Springer-Verlag, Berlin, 1975.

[19]Melnik, R. E., Chow, R. R., Mead, H. R., and Jameson, A., "An Improved Viscid/Inviscid Interaction Procedure for Transonic Flow Over Airfoils," Grumman Research Department Rept. RE-682, March 1984.

[20]Kemp, W. B., Jr., "A Slotted Test Section Numerical Model for Interference Assessment," AIAA Paper 84-0627, March 1984.